JOURNAL OF GEOPHYSICAL RESEARCH: SOLID EARTH, VOL. 118, 432–446, doi:10.1029/2012JB009527, 2013

An integration to optimally constrain the thermal structure of oceanic lithosphere

B. Goutorbe[1] and J. K. Hillier[2]

Received 13 June 2012; revised 15 November 2012; accepted 28 November 2012; published 31 January 2013.

[1] The evolution through time of the oceanic lithosphere is a substantial, incompletely resolved geodynamical problem. Consensus remains elusive regarding its thermal structure, physical properties, and the best model through which to unify observational constraints. We robustly reevaluate all three of these by (i) simultaneously fitting heat flow, bathymetry, and temperatures derived from a shear velocity model of the upper mantle, (ii) using the three main thermal models (half-space, plate, and Chablis), and (iii) analyzing five depth-age curves, wherein contrasting techniques were used to exclude anomalous features from seafloor depths. The thermal models are updated to all include a temperature-dependent heat capacity, a temperature- and pressure-dependent thermal conductivity, and an initial condition of adiabatic decompression including melting. The half-space model, which lets the lithosphere thicken indefinitely, cannot accurately fit the subsidence curves and requires mantle potential temperatures, T_m, that are too high. On the other hand, the models including a mechanism of basal heat supply are able to simultaneously explain all observations within two standard errors, with best-fitting parameters robust to the choice of the filtered bathymetry curve. For the plate model, which imposes a constant temperature at a fixed depth, T_m varies within 1380–1390°C, the equilibrium plate thickness a within 106–110 km, and the bulk thermal expansivity $\bar{\alpha}$ within $2.95-3.20 \cdot 10^{-5}$ K^{-1}. For the Chablis model, which prescribes a fixed heat flow at the base of a thickening lithosphere, the best-fitting values are $T_m = 1320-1380$°C, $a = 176-268$ km, $\bar{\alpha} = 3.05-3.60 \cdot 10^{-5}$ K^{-1}. Driven by more accurate ocean depths, the plate model provides better joint-fittings to the observations; however, it requires values of $\bar{\alpha}$ lower than experimentally measured, which can be explained by a reduction of the apparent expansivity due to elastic rigidity of the upper lithosphere. The Chablis model better fits the data when $\bar{\alpha}$ is set close to or above the experimental values. Although statistically consistent within two standard errors, a tendency toward incompatibility between observed depth-age curves and seismically derived temperatures is revealed with new clarity, because the latter do not exhibit a clear steady state whereas the former flatten; further work is needed to identify the origin of this apparent discrepancy.This work opens the way to investigations fully independent of particular solutions of the heat equation.

Citation: Goutorbe, B., and J. K. Hillier (2013), An integration to optimally constrain the thermal structure of oceanic lithosphere, *J. Geophys. Res. Solid Earth*, *118*, 432–446, doi:10.1029/2012JB009527.

1. Introduction

[2] The thermal structure and evolution of the oceanic lithosphere is a central problem of geodynamics, which is directly linked to the style of plate tectonics, the global heat loss of the Earth, and the mechanisms of lithosphere-asthenosphere interaction. Subsidence of the ocean floor away from mid-ocean ridges is well explained by the cooling of a thermal boundary layer [*Turcotte and Oxburgh*, 1967]; the lithosphere is hot when created at mid-oceanic ridges then cools primarily by conduction [e.g., *Lister*, 1974; *Parsons and Sclater*, 1977], consequently contracts, becomes denser, and subsides due to isostasy [*Pratt*, 1859] as it moves away from the ridge. The detail within this model, and the fundamental question of what physical process may act to limit the growth of this uppermost boundary layer, however, remain incompletely addressed. Principally, debate concerns the existence of, and explanation for, "flattening" of the seafloor at old ages, where depths are shallower than expected from the simplest half-space cooling model [*Davis and*

[1]Instituto de Geociências, Universidade Federal Fluminense, Niterói, Brazil.
[2]Department of Geography, Loughborough University, Leicestershire, UK.

Corresponding authors: B. Goutorbe, LAGEMAR, Instituto de Geociências, Universidade Federal Fluminense, Avenida General Milton Tavares de Souza s/n, 22210-340 Niterói, Brazil. (brunog@id.uff.br)
J. K. Hillier, Room NN.1.11.e, Martin Hall, East Park, Department of Geography, University of Loughborough, Leicestershire, UK, LE11 3TU. (j.hillier@lboro.ac.uk)

2169-9313/13/2012JB009527

Lister, 1974]. Explanations are either "thermal" where heat is added, "dynamic" where the asthenosphere pushes upwards, or "chemical" where mantle mineralogy is altered to less dense forms [*McNutt*, 1995]. The thermal models are considered here.

[3] Gravity [*McKenzie*, 1967; *DeLaughter et al*., 1999] and crustal thickness [*Hillier and Watts*, 2005] have been used to constrain thermal contraction models, but surface heat flow and ocean depths are usually considered to serve as the more powerful constraints [e.g., *Parsons and Sclater*, 1977; *Stein and Stein*, 1992; *Doin and Fleitout*, 1996; *Hillier and Watts*, 2005]. Recently, tomographic estimates of seismic velocity in the upper mantle have also been employed as a proxy for temperature within the lithosphere [e.g., *Ritzwoller et al*., 2004; *Zhong et al*., 2007; *Goutorbe*, 2010]. Arguably, additional observations allow the models to be evaluated better. In particular, *Goutorbe* [2010] assessed the joint fit of the half-space, plate, and Chablis models to observed heat flow, ocean depths, and temperatures derived from the upper mantle shear velocity model of *Shapiro and Ritzwoller* [2002].

[4] Fit to the geophysical observables is achieved by allowing variation in the parameters of the lithospheric models and selected thermophysical properties of the lithosphere. *Parsons and Sclater* [1977], for instance, fixed what they considered the then best constrained properties (i.e., density, heat capacity, and thermal conductivity of the mantle) and inverted for basal temperature, plate thickness, and thermal expansivity. Simpler inversions use depth-integrated "bulk" values [e.g., *Parsons and Sclater*, 1977; *Stein and Stein*, 1992; *Hillier and Watts*, 2005], while others improve upon this by using temperature and/or pressure dependent experimentally constrained values [e.g., *Denlinger*, 1992; *Doin and Fleitout*, 1996] and by taking into account the adiabatic gradient within the initial temperature condition [*McKenzie et al*., 2005; *Goutorbe*, 2010]. Values of parameters that best fit observations vary because of this. The principal thermal models are the half-space cooling model [*Davis and Lister*, 1974], the plate model [*McKenzie*, 1967], and the Chablis model [*Crough*, 1975; *Doin and Fleitout*, 1996]. However, these have not yet been formulated in a self-consistent way, hindering exact comparison of the models and implications of their best fit parameters and physical properties. Specifically, in their formulation *Doin and Fleitout* [1996] incorporated temperature-dependant properties within the plate and Chablis models, but used an initial condition of uniform temperature. *McKenzie et al*. [2005] included the effect of adiabatic decompression melting in the initial condition, but they only worked with the plate model, and they adjusted its parameters to get as close as possible to the GDH1 plate model [*Stein and Stein*, 1992] rather than to fit the geophysical observables. Finally, *Goutorbe* [2010] did not define the basal condition of the Chablis model in a manner that took into account the adiabatic gradient.

[5] Another improvement consists of selecting the observations that most faithfully represent the thermal structure of the lithosphere; ocean depths, for example, are in many areas obscured by perturbations unrelated to "plate-scale" lithospheric cooling [*Hillier and Watts*, 2005] such as those caused by anomalous crust or dynamic topography. This has motivated several recent works focused on filtering out anomalous seafloor in order to isolate the plate-scale trend of subsidence [*Hillier and Watts*, 2004, 2005; *Crosby et al*., 2006; *Zhong et al*., 2007; *Korenaga and Korenaga*, 2008].

[6] The present work reevaluates the models that approximate the thermal evolution of oceanic lithosphere by integrating several aspects of current best-practice, specifically (i) simultaneously fitting heat flow, bathymetry and temperatures derived from a shear velocity model of the upper mantle, (ii) using a self-consistent implementation of the three main thermal models with temperature-dependent thermophysical properties and including continuity to depth (up to 160km), and (iii) analyzing five independently obtained depth-age curves. This is the first use of entirely self-consistent implementation of all the main thermal models in the context of an inversion for lithospheric properties. The objectives are (1) to determine whether or not the plate and Chablis models are materially different in the implications of their formulation and expectations of plate thickness and mantle temperature, (2) to evaluate the sensitivity of these to bathymetry selection methodology, and (3) to reevaluate the necessity for invoking rigidity in the upper lithosphere [as *Pollack*, 1980; *Korenaga*, 2007] to explain plausibly determined but large reductions in effective values of expansivity found in most previous studies [*Parsons and Sclater*, 1977; *Stein and Stein*, 1992; *Hillier and Watts*, 2004; *Goutorbe*, 2010].

2. Data

[7] Three classes of constraints upon the thermal structure of the oceanic lithosphere are constructed from geophysical observables:

1. Mean surface heat flow, $\bar{q}(t) \pm 2\sigma_{\bar{q}}(t)$,
2. Mean ocean depths, $\bar{d}(t) \pm 2\sigma_{\bar{d}}(t)$,
3. Mean temperatures derived from a shear velocity model of the upper mantle, $\bar{T}(z,t) \pm 2\sigma_{\bar{T}}(z,t)$,

where t is the age of the oceanic lithosphere and z is depth below the seafloor (see Table 1). $\bar{q} \pm 2\sigma_{\bar{q}}$ versus t is illustrated in Figure 1a, $\bar{d} \pm 2\sigma_{\bar{d}}$ versus t in Figure 1b, and $\bar{T} \pm 2\sigma_{\bar{T}}$ versus z at two fixed t in Figure 1c; in addition, Figure 1d shows the depth of the 1100°C isotherm of the seismically derived temperature field $\bar{T}(z,t)$, versus t. The steps applied to derive $\bar{q}, \bar{d}$, and $\bar{T}$ are outlined below.

[8] As Figure 1 indicates, five sets of constraints are created. Each set includes d, q, and T data, but each is formulated around a different bathymetry grid. These are the bathymetries produced by applying one of the recently proposed techniques to filter out anomalous ocean depths (Table 2), which will be assessed in more detail in section 2.1. The bathymetry grids, however, cover different spatial extents ranging from the North Pacific to the global ocean, and they can exclude subareas where ocean depths are considered anomalous. The extents of q and T data are different again. Therefore, for each set of constraints, q and T data are resampled to include only data from areas where there is bathymetry. In this, it is also necessary to account for differing spatial resolutions of the data sets.

[9] The global databases of heat flow measurements q and temperatures derived from seismic tomography T are the same as in *Goutorbe* [2010]; specifically, we have at our disposal 14,400 oceanic heat flow measurements and their point

Table 1. Table of Notation

Symbol	Quantity	Unit	Reference/Note
z	Depth below seafloor	km	
t	Age of seafloor	Myr	*Müller et al*. [2008]
$\bar{q} \pm \sigma_{\bar{q}}$	Mean heat flow and standard error	mW m^{-2}	Observational constraint
$\bar{d} \pm \sigma_{\bar{d}}$	Mean depth of seafloor and standard error	km	Observational constraint
$\bar{T} \pm \sigma_{\bar{T}}$	Mean temperature derived from seismic tomography and standard error	°C	Observationally-derived constraint
T_m	Mantle potential temperature	°C	Free parameter of the thermal models
a	Asymptotic plate thickness	km	Free parameter of the thermal models
$\bar{\alpha}$	Bulk thermal expansivity	K^{-1}	Free parameter of the thermal models
ρ_{water}	Density of seawater	kg m^{-3}	1000 kg m^{-3}
ρ_0	Density of mantle at 0°C	kg m^{-3}	3330 kg m^{-3}
ρ	Mantle density	kg m^{-3}	$\rho(T) = \rho_0 \cdot \exp\left(-\int_{T_0}^{T} \alpha(T')dT'\right)$ [a]
λ	Mantle thermal conductivity	Wm^{-1} K^{-1}	$\lambda(P,T)$ from *Hofmeister* [1999]
c_P	Mantle heat capacity	J kg^{-1}K^{-1}	$c_P(T)$ from *Berman and Aranovich* [1996]
T	Temperature	°C	
P	Pressure	MPa	Lithostatic pressure, derived from PREM density model
s_T	Misfit to temperatures	–	Equation (6)
s_d	Misfit to depths	–	Equation (8)
s_q	Misfit to heat flow	–	Equation (7)
s	Joint misfit	–	Equation (9)

[a]Reduces to $\rho(T) = \rho_0 \cdot \exp[-\bar{\alpha}(T - T_0)]$ with a bulk, constant thermal expansivity $\bar{\alpha}$.

locations. These are from the global compilation of *Pollack et al*. [1992], updated for data until 2010 by F. Lucazeau and D. Hasterock (personal communication, 2010). To make spatial extents consistent, we retain only the measurements falling within cells containing seafloor depth values for the bathymetry grid under consideration. Mantle temperatures are derived at regular depths below the seafloor from the global $2° \times 2°$ upper-mantle shear velocity model of *Shapiro and Ritzwoller* [2002], using the velocity-temperature relationship of *Goes et al*. [2000]. In fact, seismic velocities are sensitive to both thermal and compositional variations in the mantle [*Yan et al*., 1989; *Sobolev et al*., 1996; *Artemieva*, 2009]; we include the latter (nonthermal) component within the final uncertainties of the seismically derived temperatures, by spanning the range of reported compositions of oceanic peridotites (e.g., *Niu et al*. [1997]; see *Goutorbe* [2010] for more details). To be retained, a tomography cell's plan view domain must contain at least one valid depth from the bathymetry grid. Because the tomography grid is coarser, this selection scheme does not guarantee the exclusion of cells affected by mantle plumes, if such things exist [*Anderson*, 2005; *Sleep*, 2006]. Since we are interested in the thermal evolution of the lithosphere irrespective of what drives it, removing temperatures in the lithosphere is not desirable; but in all rigor, one should discard asthenospheric temperatures in plume conduits because they are potentially hotter and may thus bias the inversions toward too large mantle temperatures (Figure 2). We tested the effect of removing all tomography cells within a radius of 300 km of hot spots catalogued by [*Anderson and Schramm*, 2005], and found no noticeable difference in the mean temperature trends and inversion results. Namely, the spatial and density inconsistencies of the data do not materially affect the results.

[10] The next step, for each set of constraints, consists of associating an oceanic age t with each ocean depth d, heat flow q and seismically derived temperature T. t values are from the grid of seafloor age of *Müller et al*. [2008]. This allows arithmetic averages to be calculated for the geophysical observables, $\bar{d}, \bar{q}$, and $\bar{T}$, within intervals of similar age t: for temperatures, this averaging process is further repeated at regular depths below the seafloor z. q and d are averaged within 2 Myr intervals between 0 and 160 Myr, T within 4 Myr intervals in the same range and every 4 km between 20 and 160 km below seafloor. Uncertainties associated with these averages are described with normal distributions of standard deviation $\sigma_{\bar{T}}, \sigma_{\bar{q}}$, and $\sigma_{\bar{d}}$, respectively (see section 2.2). Heat flow measurements on seafloor younger than 50 Myr are discarded from the fits because hydrothermal circulation is likely to add a systematic advective component [e.g., *Stein and Stein*, 1994; *Elderfield et al*., 2004].

2.1. Depth-age Curves

[11] It is essential that depth data are selected so that they are consistent with any thermal model of the lithosphere later fitted to them. Sediment loading, for instance, is always corrected. Ocean depths include features typically argued to be unrelated to "plate-scale" lithospheric cooling such as seamounts, oceanic islands and plateaus, and "hot spot" swells [e.g., *Heestand and Crough*, 1981; *Hillier and Watts*, 2005]. Such features arguably reflect anomalous crust, hotter asthenosphere and/or dynamic topography, and it therefore appears essential to remove them when deriving a depth-age curve suitable to constrain a thermal model based on monotonically progressing lithospheric cooling (Figure 2). Alternatively, a model including stochastic lithospheric reheating, such as proposed by *Smith and Sandwell* [1997], may retain swells, considering them thermally supported [e.g., *Detrick and Crough*, 1978; *Marks and Sandwell*, 1991]. However, the argument is nuanced [e.g., *Hillier and Watts*, 2005], particularly for swells and superswells [e.g., *McNutt*, 1998]. Swells are created by "thermal" support through lithospheric reheating [e.g., *Crough*, 1978] or "dynamic" support in the form of active upwelling causing upward stresses on the base of the lithosphere, reflecting asthenospheric thermal structure [e.g., *Watts et al*., 1985; *Moore and Schubert*, 1997]. The latter

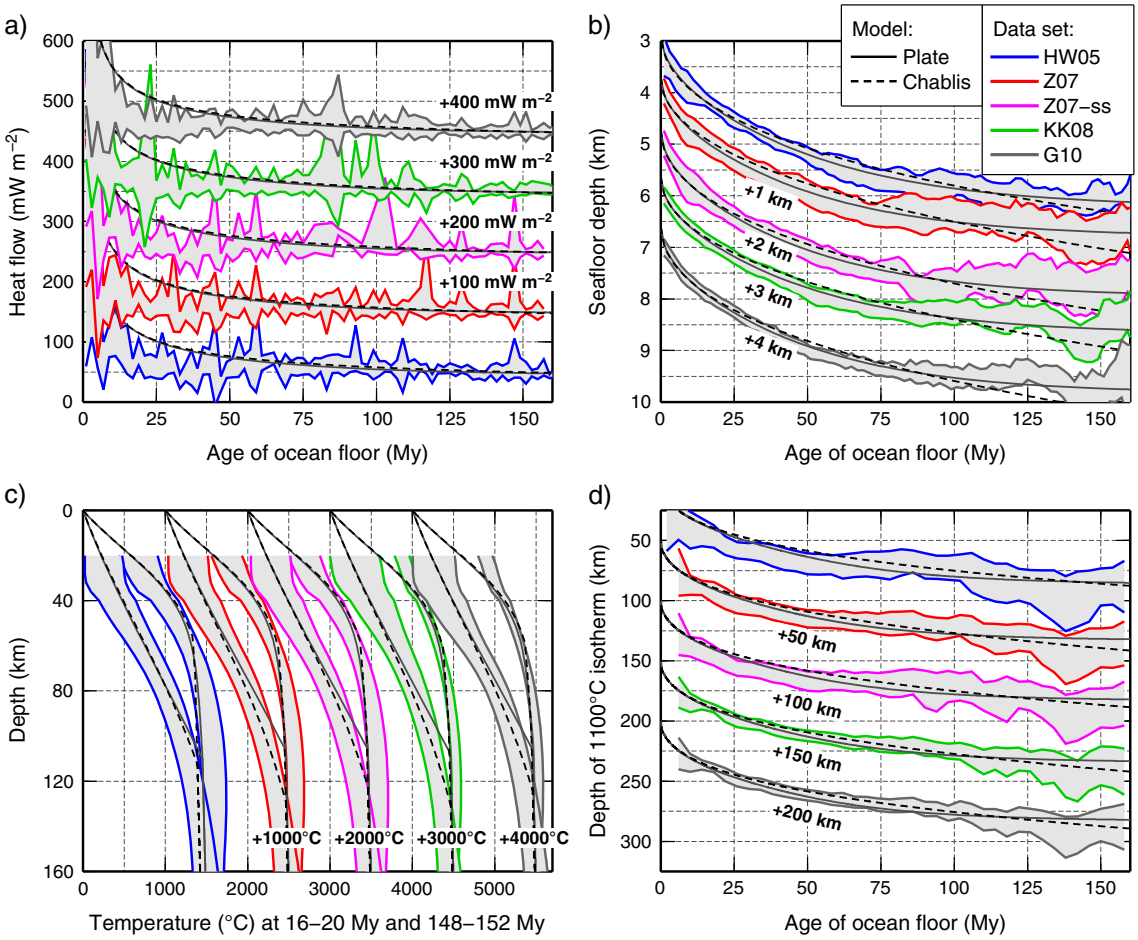

Figure 1. Data and best fitting plate and Chablis models. Shaded areas are two standard errors around (a) the mean heat flow, (b) the mean seafloor depths, (c) the mean seismically derived temperatures, and (d) the depth of the 1100 °C isotherm of that temperature field. Each data set is based on one of the published bathymetry grids described in Table 2. Heat flow measurements and seismically derived temperatures, which fall within the spatial extent of the bathymetry grid, are extracted from the global databases at our disposal. Data are then averaged within intervals of similar age of ocean floor (see section 2 for details).

presumably fades as volcanism ceases; the former lingers [e.g., *Smith and Sandwell*, 1997; *Thoraval et al*., 2006; *Asaadi et al*., 2011] but reduces in amplitude, and can become difficult to distinguish. For instance, even old Pacific volcanic groups can coexist with spatially correlated topographic rises [*Hillier and Watts*, 2005], but it is often still unclear to what extent these are thermal remnants as opposed to being chemical in origin (e.g., underplating [*Caress et al*., 1995; *McNutt*, 1998] or supported by remnant depleted material [*Jordan*, 1979]). Depth data have therefore been handled in a variety of ways.

[12] Early works manually selected localities "well-known" to be unperturbed [e.g., *Sclater et al*., 1971; *Parsons and Sclater*, 1977]. Some more recent model-fitting studies have applied simple filtering schemes, if any at all, to global

Table 2. Bathymetry Grids Included in the Present Work

Reference(s)	Extent	Abbrev.	Filtering Method
Hillier and Watts [2004, 2005]	North Pacific[a]	HW05	Regional-residual separation algorithm
Zhong et al. [2007]	Pacific[b]	Z07	Removal of seamounts (identified by gravity data) and large igneous provinces
Zhong et al. [2007]	Pacific[c]	Z07-ss	*Idem*, excluding Hawaiian and South Pacific superswells
Korenaga and Korenaga [2008]	All oceans	KK08	Exclusion based on distance criterion
Goutorbe [2010]	All oceans	G10	Exclusion of depths more than 600 m shallower than the median value within 2 Myr age intervals

[a]Data used to generate their curve iv [see *Hillier and Watts*, 2005, Figure 6].
[b]Their Figure 4b.
[c]Without Hawaiian and South Pacific superswells (their Figure 10b).

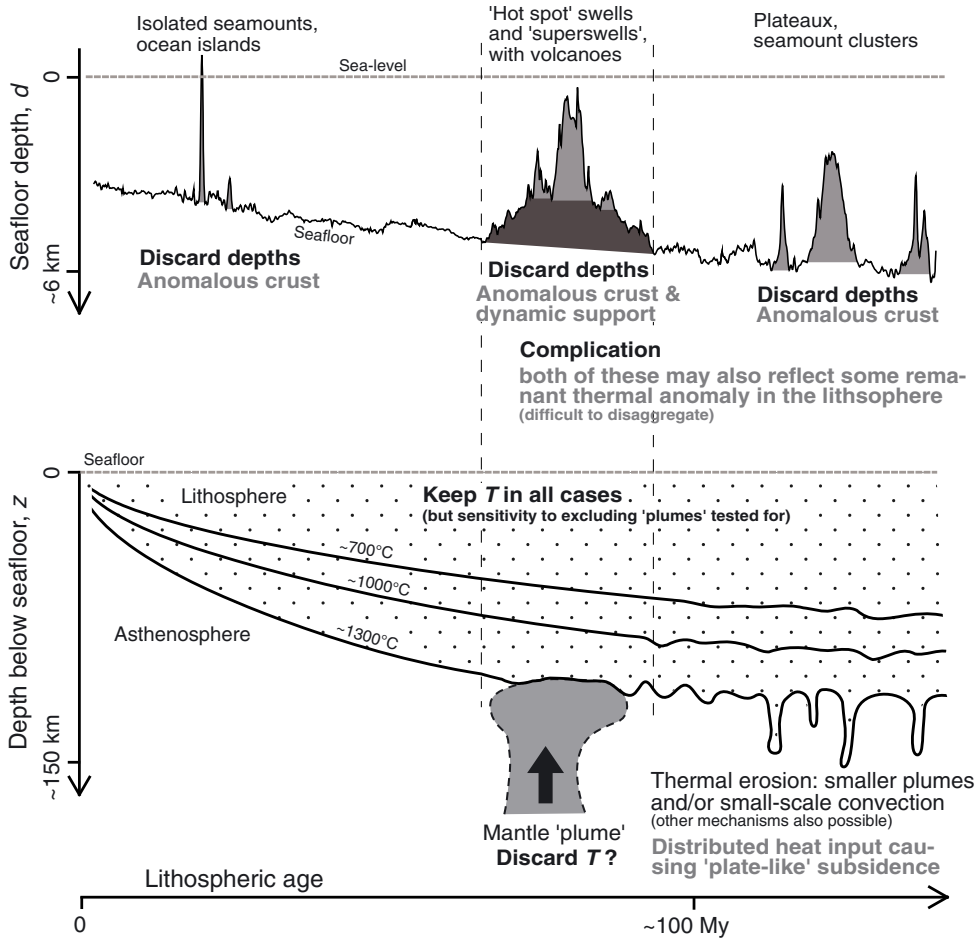

Figure 2. Illustration of the philosophy behind the selection of ocean depths and seismically derived temperatures which, for both, is to discard (or interpolate under) features that dominantly reflect effects unrelated to the thermal structure of the lithosphere such as anomalous crustal thickness, hotter asthenosphere or dynamic topography (see text, section 2). Note that the selected data record the thermal erosion induced by mantle plumes and/or small-scale convection, if such things exist. Numbers given are indicative, typical values.

bathymetry grids [*Stein and Stein*, 1992; *Doin and Fleitout*, 1996; *Goutorbe*, 2010], which did not guarantee the complete exclusion of unwanted features. Since 2004 several studies have independently brought fresh perspectives to this problem by introducing more sophisticated filtering methods devised to extract depth-age curves that are believed to more accurately represent the conductive thermal structure of the lithosphere. We included five curves in this study, which are shown in Figures 1b and 3, and listed in Table 2.

[13] *Hillier and Watts* [2004, 2005] (HW05) applied in the North Pacific a regional-residual separation algorithm, inspired by manual identification of anomalous features along bathymetric profiles, which tends to pass under rather than through small- and medium-scale edifices such as oceanic plateaus. They individually justify removing each medium-scale topographic high. In a thermal model where plumes are postulated to flatten seafloor at old ages, or basal heat supply in the plate model is provided this way, this curve may be too deep by the size of whatever thermal perturbation remains in medium-scale rises associated with oceanic islands. Often the deepest possible, this curve is the least likely to show flattening. The removal or otherwise of swells, particularly Hawaii, is contentious [see *Hillier and Watts*, 2005] and can lead to apparent temporary shallowing (~90–120 Myr) if incompletely done. However, recent work [e.g., *Crosby et al*., 2006; *Asaadi et al*., 2011] tends toward a dominantly convective, dynamic origin of the Hawaiian Swell, and no topographic expression of nearby (i.e., not far field) balancing downwelling has been reported. Therefore, curve iv of *Hillier and Watts* [2005], which removes the Hawaiian Swell, is selected here (Table 2). Although debate exists [*Adam and Bonneville*, 2005], the Pacific superswell probably does not impinge on the North Pacific [e.g., *McNutt and Judge*, 1990; *McNutt*, 1998; *Hillier and Watts*, 2004].

[14] *Zhong et al*. [2007] (Z07) removed, in the Pacific, large igneous provinces delimited by *Coffin and Eldholm* [1994], and seamounts identified from gravity data by *Wessel* [2001]; they also present in their Figure 10b an alternative bathymetry curve obtained from areas that avoid the Hawaiian swell and South Pacific superswell (Z07-ss), suppressing the shallowing between ~80–120 Myr originating there.

[15] *Korenaga and Korenaga* [2008] (KK08) define as anomalous regions where bathymetry is shallower than the plate model of *Stein and Stein* [1992] by more than 1000 m. They then produce global bathymetry grids by excluding

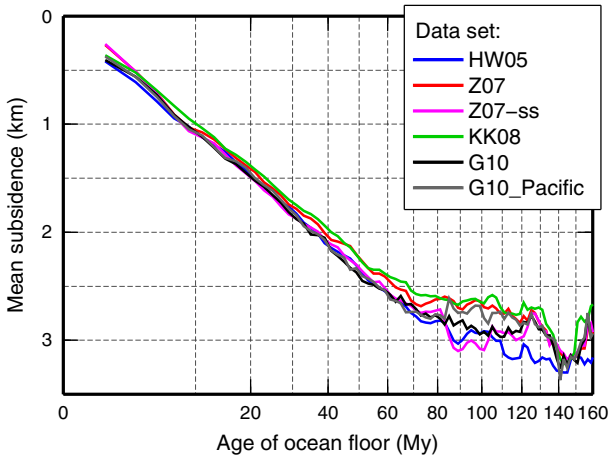

Figure 3. Mean subsidence relative to zero-age depth, versus age of ocean floor (square root scale). Gray curve corresponds to the bathymetry grid of G10 [*Goutorbe*, 2010] restricted to the Pacific.

these anomalous ocean depths and seafloor in their vicinity, based on a distance criterion and a correlation criterion: we use a grid generated using the former criterion.

[16] Finally, for continuity, and as a second global estimate we include the curve of *Goutorbe* [2010] (G10) who simply, at a global scale, excluded depths more that 600 m shallower than the median value within each 2 Myr age interval.

[17] The depth-age curves as showed in Figure 1b appear slightly different from the originally published curves, because (1) we recalculate the mean depths using the age grid of *Müller et al*. [2008] and (2) we use as error bars the 2σ uncertainty of the means, described in section 2.2, rather than the standard deviations. When aligned according to their zero-age depth, the curves appear broadly similar in the part showing linear dependence against $\sqrt{\text{age}}$, that is, from 0 Myr up to at least ~60 Myr (Figure 3). Following *Hillier and Watts* [2005], zero-age "ridge" depth is estimated from a linear regression of bathymetry against $\sqrt{\text{age}}$, in this work within 0–60 Myr. Differences are mostly visible where the subsidence curves flatten. Here, seafloor has existed longer to be perturbed, and less remains, making 'normal' seafloor more difficult to determine. HW05 exhibits the smoothest behavior, monotonically approaching an asymptotic subsidence of about 3.2 km. It is difficult to identify clear asymptotic values for the other curves. Z07-ss explicitly avoids major features suspected to be dynamic in origin (e.g., Hawaiian swell, Pacific superswell) and subsides similarly to HW05, but is shallower after ~110 Ma. Since it is similar in shape to Z07, which explicitly retains the Pacific superswell and the Hawaiian swell, it seems that KK08 does not discard entirely these dynamic features. Therefore, because they remove the long wavelength swells, the HW05 and Z07-ss data sets appear better suited to an exercise fitting a thermal cooling model of the lithosphere. The global scale G10 curve resembles HW05 and Z07-ss but, interestingly, a subset of data from G10 for the Pacific appears significantly shallower between 80–120 Myr, making it closer to Z07 and KK08. This suggests that the large-scale anomalous features encountered in the Pacific resist simpler filtering methods.

2.2. Uncertainties of the Means

[18] Since the errors on the data are unlikely to be spatially independent, the uncertainties of the means, $\sigma_{\bar{T}}$, $\sigma_{\bar{q}}$ and $\sigma_{\bar{d}}$, are evaluated within each age interval following *Goutorbe* [2010], that is, taking into account the correlation of the errors: $\sigma_{\bar{x}} = \left(\sum w_i\right)^{-2} \cdot \sum w_i w_j \operatorname{cov}\left(x_i, x_j\right)$, where w_i represents a latitude-dependent area weighting (or = 1 in the case of heat flow data) and x one of the three data classes. Based on the sample autocorrelation plots, an exponential covariance function with a correlation distance $\delta = 1000$ km for temperatures and ocean depths, and $\delta = 50$ km for heat flow measurements, is chosen [*Goutorbe*, 2010]:

$$\operatorname{cov}\left(x_i, x_j\right) = \left[\operatorname{var}(x) + \sigma_{x_i}\sigma_{x_j}\right] \exp\left(-\frac{\operatorname{dist}\left(x_i, x_j\right)}{\delta}\right), \qquad (1)$$

with var(x) the variance within an age interval and σ_{x_i} the individual data uncertainties. Following *Goutorbe* [2010], the uncertainties in temperature σ_{T_i} are estimated from a stochastic error propagation, which includes uncertainties on the thermo-elastic properties, on mantle composition, on the anelastic factor and on seismic velocities: typically, $\sigma_{T_i} \approx 100-150°\text{C}$, and $\sigma_{\bar{T}} \approx 30-80°\text{C}$ (global extent) to 60–120°C (North Pacific only). A simple and general method has to be adopted to affect individual uncertainties σ_{q_i} to heat flow measurements, since such information is rarely reported in our global database. From available values, which are assumed to represent the 2σ uncertainties (or 95% confidence intervals), we find a median relative uncertainty around 0.1: we generalize this by affecting $\sigma_{q_i} = 0.05 \times q_i$. Finally, the correction for sediment load being the main source of error for ocean depths, we take $\sigma_{d_i} = 0.1 \times$ sediment thickness (Laske, personal communication, 2009). The grid of sediment thickness is taken from *Laske and Masters* [1997] for G10, and from the NGDC [*Divins*, 2011] for other curves. In Figures 1a–1c, gray areas show $2\sigma_{\bar{x}}$ around the means, which approximately correspond to the 95% confidence interval of the means since normal distributions are used.

3. Thermal Models, Parameters, and Misfit

[19] This work assesses the three main thermal cooling models as means of which approximating the thermal structure and evolution of the oceanic lithosphere. These, however, can be formulated in slightly varying ways, which causes different thermal structures to be determined even when the same physical parameters are used (Figure 4). Calculations here are based on the work of *Goutorbe* [2010] and use variable material properties as is now common practice [*Doin and Fleitout*, 1996; *Honda and Yuen*, 2001; *Korenaga and Korenaga*, 2008], but a number of methodological adjustments have been made in order to integrate the thermal models and synthesize best practice. For convenience, and to contextualize the detailed description that follows, we summarize these here.

[20] First, and for the first time, we modify the Chablis model so that the base of the lithosphere is defined consistently with an adiabatic temperature profile, rather than at a fixed temperature (section 3.1) [*Crough*, 1975; *Doin and Fleitout*, 1996]. Second, the misfit to seismically derived temperatures is calculated over the whole depth range of the T data, rather than over just the depth range of the lithosphere as defined by the models (section 3.2). Third, *Goutorbe* [2010] offset

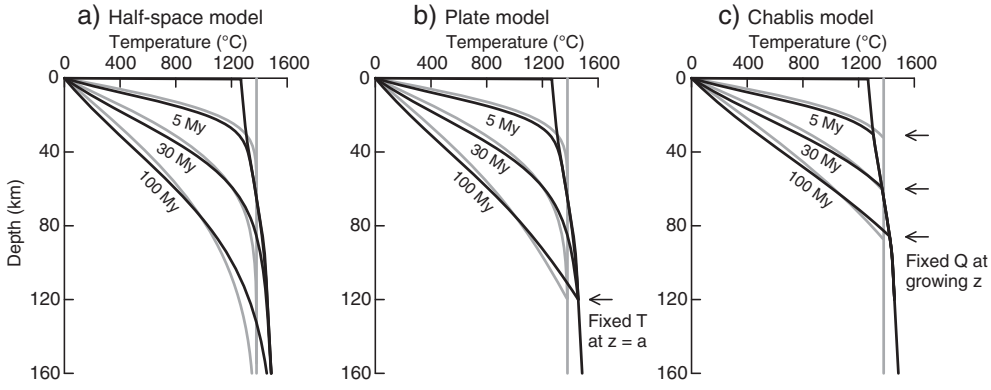

Figure 4. Examples of modeled temperature fields illustrating the influence of model formulation. Grey lines are for simpler thermal models with constant properties and uniform initial temperature (thermal diffusivity $\lambda/\rho c_P = 8 \cdot 10^{-7}$ m^2 s^{-1}, initial and basal temperature = 1380°C, plate thickness = 120 km). Black lines are for the thermal models used in this paper. Parameters include the temperature and/or pressure dependencies described in the text. The initial temperature profile corresponds to an adiabatic upwelling with anhydrous decompression melting, as parameterized by *Katz et al*. [2003]; it also provides a physical rationale for extending the temperature field below the base of the plate and Chablis models. The same parameters are used for all models: potential temperature of the mantle $T_m = 1380$°C and (for the plate and Chablis models) equilibrium plate thickness $a = 120$ km. The initial temperature profile intersects a value slightly lower than T_m at the surface because of the effect of latent heat of fusion.

the modeled subsidence according to the difference with the observed bathymetry within the lowest age interval, whereas we use here the ridge depth estimated from a linear regression of bathymetry against $\sqrt{\text{age}}$ (sections 3.1) [e.g., *Hillier and Watts*, 2005]. Fourth, the third adjustable parameter of the thermal models used is the bulk expansivity $\bar{\alpha}$, rather than the reduction of $\alpha(T)$ below 1000°C, for the reasons exposed in section 3.3

3.1. Three Classes of Model

[21] The thermal evolution models, $T_{mod}(z,t)$, are solutions of the one-dimensional heat equation,

$$\rho c_P \frac{\partial T}{\partial t} = \frac{\partial}{\partial z}\left(\lambda \frac{\partial T}{\partial z}\right), \tag{2}$$

with temperature- and pressure-dependent mantle properties: thermal conductivity $\lambda(P,T)$ from *Hofmeister* [1999] and heat capacity $c_P(T)$ from *Berman and Aranovich* [1996]. Mantle density ρ is 3330 kgm^{-3} at surface conditions, and varies with temperature, but by at most a few percent. These variations have a negligible effect on the temperature field, but cause the modeled subsidence.

[22] *Katz et al*. [2003] parameterized the temperature variation of an adiabatically upwelling mantle with melt production at constant entropy, which is used as initial condition. This temperature profile depends on the potential temperature of the mantle T_m, which is left as a free parameter, and the weight fraction of water and modal clinopyroxene, which are set to 0% and 10%, respectively. The top boundary condition is $T_{mod}(0,t) = 0$°C. The three classes of model we consider essentially differ by their bottom condition:

1. The half-space model does not prescribe any basal boundary condition, so that the cold temperature imposed at the surface diffuses down indefinitely (Figure 4a) [*Davis and Lister*, 1974].
2. The plate model imposes a constant temperature at a fixed depth a, which prevents the lithosphere from thickening indefinitely [*Parsons and Sclater*, 1977]. In order to be consistent with the initial condition, the basal temperature is the value at depth a of the adiabatic decompression melting profile with potential temperature T_m as parameterized by *Katz et al*. [2003] (Figure 4b). In the plate model, heat is supplied to the base of the lithosphere at old ages, which can be interpreted as an approximation of the effect of convective instabilities starting to develop at a critical age [*Parsons and McKenzie*, 1978; *Davaille and Jaupart*, 1994; *Huang and Zhong*, 2005].
3. It may be argued that basal heat supply from convective processes actually occurs at all ages: this leads to the Chablis model, which imposes a constant heat flow Q_m at the base of a growing boundary layer [*Crough*, 1975; *Doin and Fleitout*, 1996]. Previous works defined such a layer as increasing in thickness whenever a node fell below a fixed temperature. Consistency with the initial condition here modifies this to use the adiabatic decompression melting profile of potential temperature T_m instead of a fixed temperature (Figure 4c). Everything else being equal, there is a one-to-one correspondence between Q_m and the asymptotic thickness a of the boundary layer.

[23] By construction, the parameter T_m of all the models represents the potential temperature of the mantle, and a the asymptotic thickness of the lithosphere. The temperature field of the models is numerically approximated from a finite-difference method centered in depth and explicit in time, and the base of the boundary layer of the Chablis model is tracked following the scheme proposed by *Crough and Thompson* [1976]. The temperature field of the plate and Chablis models is naturally extended below the base of the lithosphere, thanks to the adiabatic decompression melting profile which serves as initial condition (Figure 4). This implicitly assumes that the base of both models really connects

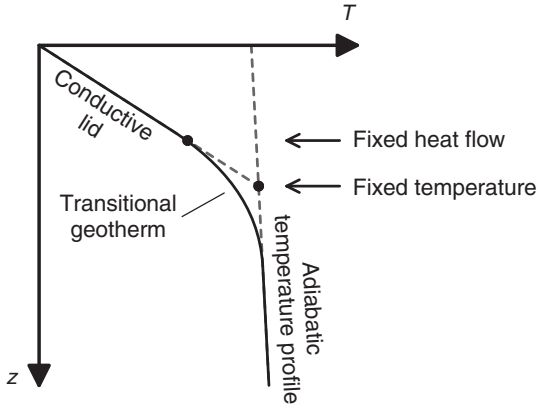

Figure 5. Proposed relationship of the basal condition of the thermal models to a conceptualization of the thermal structure of the boundary layer [from *Jaupart and Mareschal*, 2007, reprinted by permission].

to the adiabatic temperature profile of the asthenosphere. Contrastingly, *Jaupart and Mareschal* [2007] suggest that, if the fixed temperature condition indeed applies to the intersection of the downward extended conductive geotherm and the upward extended convective profile, the fixed heat flow condition rather applies to the base of the purely conductive region of the thermal boundary layer (Figure 5). However if the Chablis model is seen as not modeling the transitional geotherm, self-consistency requires either to insert it manually between the base and the adiabatic temperature profile, or to remove from the fit temperatures below the base and accordingly subtract the associated subsidence from the observed bathymetry. Without further information, both options are infeasible, and they would anyway limit the interest of the model as a consistent description of the thermal structure of the lithosphere.

[24] From a thermal model $T_{\mathrm{mod}}(z,t)$, one obtains surface heat flow $q_{\mathrm{mod}}(t)$ using Fourier's law, and subsidence relative to zero-age depth, $d_{\mathrm{mod}}(t) - d_0$, by assuming isostasy [e.g., *Pratt*, 1859; *McKenzie et al*., 2005]:

$$q_{\mathrm{mod}}(t) = \lambda \left(\frac{\partial T_{\mathrm{mod}}}{\partial z} \right)_{z=0}, \tag{3}$$

$$d_{\mathrm{mod}}(t) - d_0 \approx \int_0^a \frac{\rho[T_{\mathrm{mod}}(z,t)] - \rho[T_{\mathrm{mod}}(z,0)]}{\rho_0 - \rho_{\mathrm{water}}} \mathrm{d}z. \tag{4}$$

[25] Mantle density is evaluated as

$$\rho(T) = \rho_0 \cdot \exp[-\bar{\alpha}(T - T_0)], \tag{5}$$

where $T_0 = 0°\mathrm{C}$ is the surface temperature, $\rho_0 = 3330\ \mathrm{kg\ m^{-3}}$ the density at surface conditions and $\bar{\alpha}$ the bulk value of the coefficient of thermal expansion, which will be discussed further in section 3.3.

[26] d_0 is not simply the mean observed ridge depth, because of ridge morphological features unrelated to the thermal structure [e.g., *Malinverno*, 1990]. Given a depth-age curve $\bar{d} \pm \sigma_{\bar{d}}(t)$, d_0 is estimated from a linear regression of depths $\bar{d}$ against $\sqrt{\mathrm{age}}$, weighted by the inverse of squared uncertainties $1/\sigma_{\bar{d}}^2$, within 0–60 Myr: in this age interval, the bathymetry curves considered in the present work all exhibit a nearly linear $\sqrt{\mathrm{age}}$–depth relationship (Figure 3).

3.2. Misfit

[27] The thermal models are joint-fitted on temperature data, $\bar{T}$, heat flow data, $\bar{q}$, and bathymetry data, $\bar{d}$, by calculating the misfit s to the observations, normalized by the 2σ uncertainty of the means:

$$s_T^2(T_m, a) = \frac{1}{N_z N_t} \sum_z \sum_t \left[\frac{T_{\mathrm{mod}}(z,t) - \bar{T}(z,t)}{2\sigma_{\bar{T}}(z,t)} \right]^2, \tag{6}$$

$$s_q^2(T_m, a) = \frac{1}{N_t} \sum_t \left[\frac{q_{\mathrm{mod}}(t) - \bar{q}(t)}{2\sigma_{\bar{q}}(t)} \right]^2, \tag{7}$$

$$s_{\bar{d}}^2(T_m, a, \bar{\alpha}) = \frac{1}{N_t} \sum_t \left[\frac{d_{\mathrm{mod}}(t) - \bar{d}(t)}{2\sigma_{\bar{d}}(t)} \right]^2, \tag{8}$$

$$s^2(T_m, a, \bar{\alpha}) = \frac{1}{3} \left(s_T^2 + s_q^2 + s_{\bar{d}}^2 \right), \tag{9}$$

where the summations are performed over ages in the range $t = 50-160$ Myr for heat flow (section 2) and $t = 0-160$ Myr for ocean depths and temperatures. Due to the differences in range and interval size, the number of temperature data, N_t, is different in equations 6 to 8. Temperatures also require a summation over depths for which data are available, that is, $z = 20-160$ km below seafloor (Figure 1c): it is possible to do so because all the thermal models, which are extended downward along the adiabatic temperature profile, are defined at all depths (see section 3.1). Such a large and fixed depth range allows models to be compared against the same benchmark, and prevents models from "artificially" lowering their misfit by excluding seismically derived temperatures below their base.

[28] Because Gaussian statistics are used to describe data uncertainties, the so-defined joint misfit quantifies the overall agreement of a given thermal model with the 95% confidence interval of the averaged observations. It is calculated as a function of the free parameters of the models, namely potential temperature of the mantle T_{m}, bulk thermal expansivity $\bar{\alpha}$ and, for the plate and Chablis models, plate thickness a.

[29] The parameter space is thoroughly explored, at least sufficiently to well define all error ellipses (Figures 6 and 7), on a regular grid of step 10 °C in T_{m}, 2 km in a and $0.05 \cdot 10^{-5}\ \mathrm{K^{-1}}$ in $\bar{\alpha}$.

3.3. Thermal Expansivity as an Adjustable Parameter

[30] Even though experimental measurements of thermal expansivity are available [*Bouhifd et al*., 1996, and references therein], most previous studies included it as an adjustable parameter and found best fitting values lower than experiment: 3.11 and $3.28 \cdot 10^{-5}\ \mathrm{K^{-1}}$ in *Parsons and Sclater* [1977] (North Atlantic and North Pacific, respectively); $3.11 \cdot 10^{-5}\ \mathrm{K^{-1}}$ in *Stein and Stein* [1992]; $2.77 \cdot 10^{-5}\ \mathrm{K^{-1}}$ in *Hillier and Watts* [2005] (model X). *Pollack* [1980] and *Korenaga* [2007] explained such an observation in terms of elastic rigidity of the upper lithosphere, with the capacity to reduce the effective expansivity by up to 15% and 30%, respectively.

[31] Although some previous studies have explicitly included the temperature-dependence of expansivity as

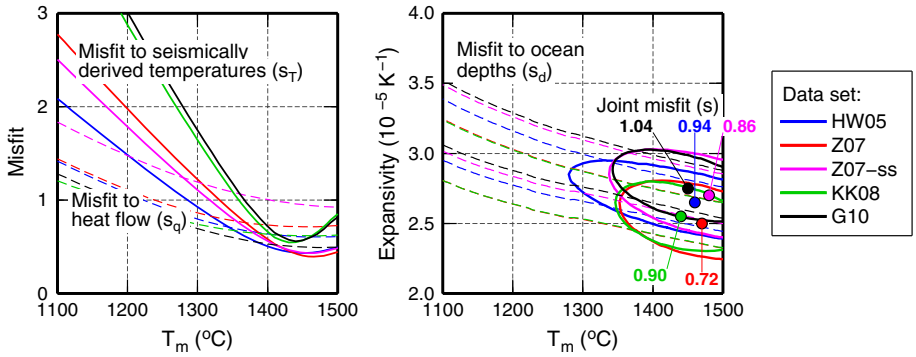

Figure 6. Misfit of the half-space model on various data sets (see Table 2), versus potential temperature of the mantle T_m and bulk expansivity $\bar{\alpha}$. (left) Misfit to heat flow s_q and misfit to temperatures s_T, versus T_m. (right) Contours of the misfit to ocean depths s_d and joint misfit s, versus T_m and $\bar{\alpha}$: value of contours is 1.2 × minimum misfits (estimated within plots limits). Labeled dots indicate the location and value of minimum misfits.

determined experimentally [*Doin and Fleitout*, 1996; *McKenzie et al.*, 2005; *Goutorbe*, 2010], we use a uniform value in equation 5. We do so for two reasons. First, numerical simulations suggest that rigidity-driven reduction itself depends on temperature [*Korenaga*, 2007, Figure 3], and so it can potentially modify the effective temperature-dependence of expansivity. Second, given a temperature field function of age and depth, we verified that the modeled

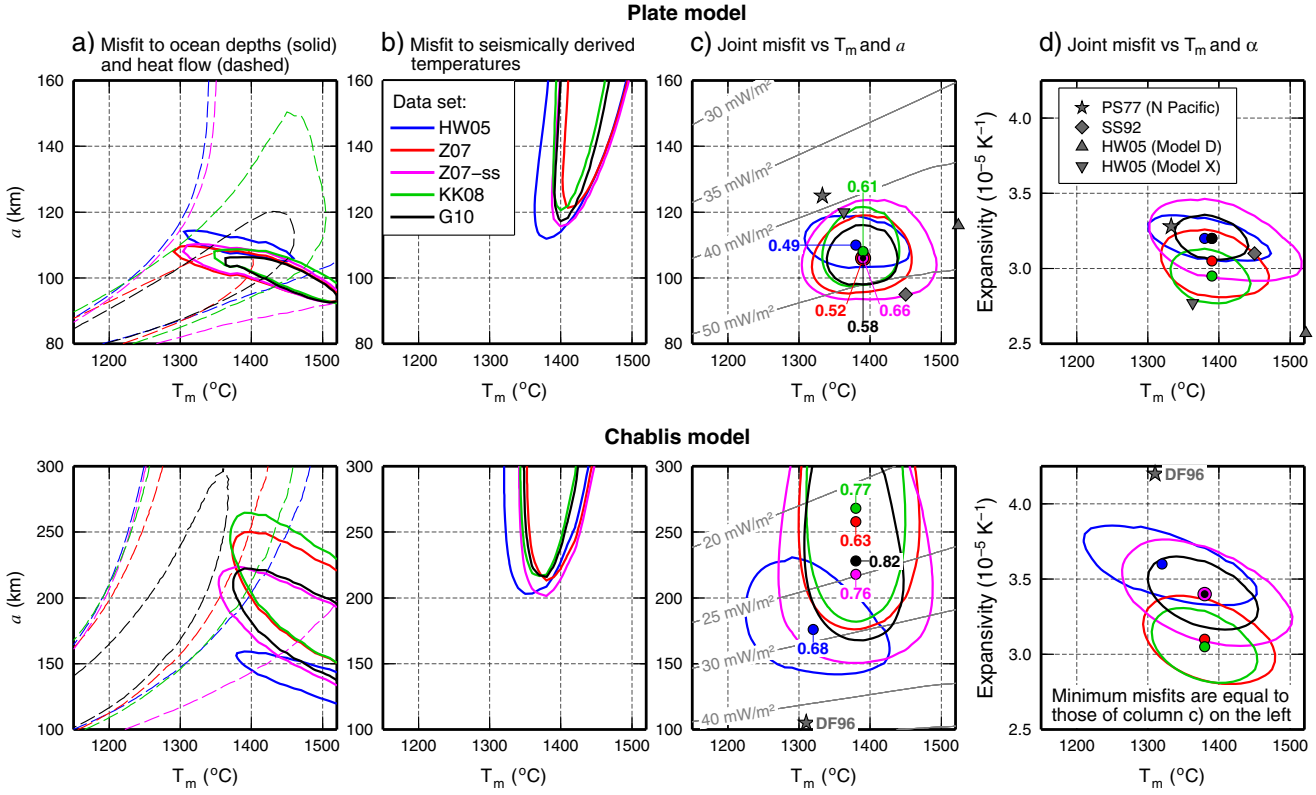

Figure 7. Misfit of the plate and Chablis models on various data sets (see Table 2), versus asymptotic plate thickness a, potential temperature of the mantle T_m and bulk expansivity $\bar{\alpha}$, in planes passing through the minimum joint misfit. Value of contours is 1.2 × minimum misfits (estimated within plots limits). Dots and labels: location and value of the minimum joint misfit. Gray lines in (c): contours of the asymptotic heat flow. Gray symbols: best-fitting parameters from some previous works: PS77: *Parsons and Sclater* [1977] (values for the North Pacific); SS92: *Stein and Stein* [1992] (GDH1 model); DF96: *Doin and Fleitout* [1996] (model 1: variable expansivity and fixed conductivity); HW05: *Hillier and Watts* [2005] (model D: variable expansivity and fixed conductivity; model X: includes 4 mW m^{-2} radiogenic heat production as PS77). These works reported basal temperature, so this is plotted rather than T_m.

Table 3. Best Fitting Parameters of the Thermal Models and Components of the Minimum Misfit. T_m: Potential Temperature of the Mantle; a: Asymptotic Plate Thickness; α: Mean Expansivity; s_T, s_d, s_q: Misfits to Seismically derived Temperatures, Ocean Depth and Heat Flow, Respectively; s: Joint Misfit

Data Set	Best Fitting Parameters			Misfit			
	T_m(°C)	a (km)	$10^5\alpha$	s_T	s_d	s_q	s
Half-space model							
HW05	1460	–	$2.65\,K^{-1}$	0.44	1.44	0.61	0.94
Z07	1470	–	$2.50\,K^{-1}$	0.40	0.94	0.72	0.72
Z07-ss	1480	–	$2.70\,K^{-1}$	0.45	1.08	0.93	0.86
KK08	1440	–	$2.55\,K^{-1}$	0.55	1.32	0.62	0.90
G10	1450	–	$2.75\,K^{-1}$	0.57	1.63	0.50	1.04
Plate model							
HW05	1380	110	$3.20\,K^{-1}$	0.54	0.27	0.60	0.49
Z07	1390	106	$3.05\,K^{-1}$	0.59	0.30	0.61	0.52
Z07-ss	1390	106	$3.20\,K^{-1}$	0.59	0.35	0.91	0.66
KK08	1390	108	$2.95\,K^{-1}$	0.78	0.45	0.55	0.61
G10	1390	106	$3.20\,K^{-1}$	0.79	0.47	0.40	0.58
Chablis model							
HW05	1320	176[a]	$3.60\,K^{-1}$	0.69	0.73	0.63	0.68
Z07	1380	258[a]	$3.10\,K^{-1}$	0.54	0.66	0.69	0.63
Z07-ss	1380	218[a]	$3.40\,K^{-1}$	0.60	0.74	0.90	0.76
KK08	1380	268[a]	$3.05\,K^{-1}$	0.74	0.94	0.60	0.77
G10	1380	228[a]	$3.40\,K^{-1}$	0.79	1.09	0.47	0.82

[a]Lithospheric thickness at 160 Myr. HW05: 115 km; Z07: 132 km; Z07-ss: 126 km; KK08: 133 km; G10: 127 km.

subsidence curve as calculated from equations 4–5 is kept virtually unmodified if we substitute an expansivity that is linearly dependent on temperature, with its age- and depth-averaged value. This means that our adjustable parameter $\bar{\alpha}$ can be interpreted as a "bulk" thermal expansivity, representative of the oceanic lithosphere as a whole, i.e., both over age and depth.

3.4. Independent Constraints on the Parameters

[32] Various studies have attempted to estimate the potential temperature of the mantle. A classical approach consists in constraining such a parameter from the geochemistry and petrology of erupted lavas. In a recent review, *Herzberg et al*. [2007] used this approach to constrain T_m as being in the range 1280–1400°C. Alternatively, *Katsura et al*. [2004] derived experimental constraints on the $P-T$ conditions of the olivine-wadsleyite phase transition, and found that for this transition to explain the seismic discontinuity at 410 km depth within the mantle, T_m should be within 1250–1350 °C.

[33] Measurements of thermal expansivity on forsterite showed a linear increase from $2.7\cdot10^{-5}$ K^{-1} at 0°C to $4.2\cdot10^{-5}$ K^{-1} at 1400 °C [*Bouhifd et al*., 1996]. For the thermal model of *Parsons and Sclater* [1977], this yields a depth-averaged lithospheric value that decreases from $4.1\cdot10^{-5}$ K^{-1} at 0 Myr to $3.5\cdot10^{-5}$ K^{-1} at 100 Myr, and an age- and depth-averaged bulk value of $\bar{\alpha}=3.6\cdot10^{-5}\,K^{-1}$. Previous studies typically found slightly larger expansivities, for example $\bar{\alpha}=3.8\cdot10^{-5}K^{-1}$ [*Gillet et al*., 1991] and $3.9\cdot10^{-5}$ K^{-1} [*Fei and Saxena*, 1986]. These bulk values do not strongly depend on the selected temperature field: in particular, using a thermal model including varying properties $\lambda(P,T), c_P(T)$ (section 3.1) has a negligible effect. Taking into account the potential reduction of the effective expansivity by up to 30 % due to elastic rigidity at low temperature [*Pollack*, 1980; *Korenaga*, 2007] allows a lower bound of $2.5\cdot10^{-5}$ K^{-1} for the effective bulk expansivity, while experimental values yield an upper bound on the order of $3.9\cdot10^{-5}$ K^{-1}.

[34] The thermal conductivity law of *Hofmeister* [1999] used in this study yields a mean value $\bar{\lambda}\approx3.3\,Wm^{-1}K^{-1}$ between 0°C and 1300°C. This is larger than the value derived from the measurements of *Schatz and Simmons* [1972], $\bar{\lambda}=3.138\,Wm^{-1}K^{-1}$, which was usually used in earlier works [e.g., *Parsons and Sclater*, 1977; *Stein and Stein*, 1992]. Recent measurements, even if they are not necessarily in exact agreement with the conductivity model of *Hofmeister* [1999], also favor a mantle thermal diffusivity larger than previously reported [*Gibert et al*., 2003, 2005].

4. Analysis of the Misfit

4.1. Half-Space Model

[35] The overall fit s of the half-space model is inferior to that of the plate and Chablis models driven by a poor fit to depth data, as $s_d\approx1$ at best (Table 3); this reconfirms that by some mechanism heat is likely supplied to the base of the lithosphere. The half-space model is best able to fit the seismic temperatures, s_T, but at the cost of a mantle temperature T_m within 1440–1480°C (Figure 6, left), which is larger than the upper bound of 1400°C derived from the independent constraints presented in section 3.4.

[36] It is possible that the excessive values of T_m are due to overly high seismically derived temperatures. To test this, an adiabatic temperature profile was fitted to the deepest seismically derived temperatures (z = 40−160 km), data most likely to be sublithospheric. The fit yielded a mantle potential temperature around ~1400°C, close to the acceptable upper bound but not demonstrably in excess of it. Some caution is necessary because this estimate has limited accuracy originating in poorly constrained anelastic effects perturbing the velocity-temperature relationship at high temperatures [*Karato*, 1993; *Goutorbe*, 2010]. The indication is, however, that the large T_m values of the half-space model are not driven by unrealistically high seismically derived temperatures in the asthenosphere. The large T_m values are actually caused by the model attempting not to fall below seismic temperatures observed beneath older seafloor. Equivalently, a still larger T_m tends to be imposed by heat flow data (Figure 6, left) as the model attempts to avoid undershooting heat flows observed on old seafloor.

[37] Because the effect of increasing T_m on the modeled subsidence can be compensated by reducing bulk expansivity $\bar{\alpha}$, there is a trade-off between these two parameters. This trade-off translates into a diagonal pattern of the misfit to ocean depths s_d (Figure 6, right). Therefore, forced to high mantle temperatures, the joint-fitting consistently yields expansivities ($\bar{\alpha}=2.5-2.75\cdot10^{-5}\,K^{-1}$) near the lower acceptable bound (section 3.4).

4.2. Thermal Models With Basal Heat Supply

[38] We now turn to the thermal models with basal heat supply. The patterns of misfit of the plate and Chablis models (Figure 7) reflect the qualitative relationships between the parameters and the observations: to a first

approximation, the asymptotic (or steady state) heat flow and thermal gradient are proportional to T_m/a, while the asymptotic subsidence is proportional to $\bar{\alpha}aT_m$ [e.g., *Stein and Stein*, 1992], leading to the orientation of the diagonal patterns in Figures 7a–7b. Regions of low misfit differ because the plate model can treat observations on old seafloor (say, older than 120 Myr) as tending to asymptotic, whilst a Chablis model with equivalent physical parameters takes about four times longer to achieve a steady state [*Doin and Fleitout*, 1996].

4.2.1. Plate Model

[39] The parameters of the plate model are remarkably consistent across the joint-fittings on the different data sets (Figures 7c–7d and Table 3).

[40] The best-fitting potential temperature of the mantle T_m is between 1380°C and 1390°C. It is thus in agreement with petrological and geochemical constraints as reevaluated by *Herzberg et al*. [2007], although close to their estimated upper bound of 1400°C (section 3.4). Such an agreement is not purely a consequence of the integration of seismically derived temperatures, which effectively force T_m a little below 1400°C, as simultaneous fits restricted to heat flow and depths also yield T_m that are consistent with independent constraints. This contrasts with previous analyses, which often found too high basal temperatures (Figure 7c, top), even after reducing them by converting to potential temperature T_m (a necessary step since the adiabatic gradient was rarely taken into account in the previous works): e.g., basal temperatures of 1450°C in *Stein and Stein* [1992] or 1522°C in *Hillier and Watts* [2005] (model D). *Parsons and Sclater* [1977] and *Hillier and Watts* [2005] (model T) attributed 4 mW m^{-2} to radiogenic heat production to lower this to 1333°C and 1490°C, respectively. Furthermore, *Hillier and Watts* [2005] had to include an observed crustal thickness of 7.1 ± 0.8 km from *White et al*. [1992] in their joint misfit to obtain a reasonable value of 1363°C (model X). The thickness was related to, and effectively forced, basal temperature through the geochemical relations of *McKenzie* [1984] or *White and McKenzie* [1995]. This additional constraint allowed them to invert for a fourth parameter, bulk thermal conductivity $\bar{\lambda}$, finding $\bar{\lambda} = 3.37\,\mathrm{Wm^{-1}K^{-1}}$. This is larger than the value typically used in earlier studies, $\bar{\lambda} = 3.138\,\mathrm{Wm^{-1}K^{-1}}$, but it agrees well with the thermal conductivity law employed in this study, which yields a mean value $\bar{\lambda} \approx 3.3\,\mathrm{Wm^{-1}K^{-1}}$ between 0°C and 1300°C (section 3.4). As T_m is on the order of $aq_\infty/\bar{\lambda}$, where q_∞ is the asymptotic heat flow, such a larger thermal conductivity is sufficient to lower T_m by ~100°C : see models L to S of *Hillier and Watts* [2005].

[41] The best-fitting plate thickness a of the plate model is also extremely stable, varying between 106 km and 110 km depending on the data set (Table 3). As expected [*Denlinger*, 1992; *McKenzie et al*., 2005], these are thinner than equivalent plates of constant properties, such as model X of *Hillier and Watts* [2005] whose plate thickness is 120 km. a and the mean thermal diffusivity $\bar{\kappa}$ naturally define a conduction timescale $\tau = a^2/\bar{\kappa}$, which gives an order of magnitude for the age of flattening. Therefore, the subsidence curve that flattens on the oldest seafloor, HW05 (Figure 3), translates into a slightly thicker plate. The best fitting a and T_m correspond to an interval of 45−47 mW m^{-2} for the steady state heat flow, in line with the measurements at old ages (Figure 1c). It is understandably a little higher than predicted by the thermal models of *Parsons and Sclater* [1977] and *Hillier and Watts* [2005, model X] selected in Figure 7c, because these invoked radiogenic heat production to reduce the observed heat flow attributable to cooling by 4 mW m^{-2}.

[42] Like T_m and a, the mean expansivity $\bar{\alpha}$ of the plate model covers a limited range across the joint-fittings, from $2.95 \cdot 10^{-5}$ K^{-1} to $3.20 \cdot 10^{-5}$ K^{-1} (Figure 7d and Table 3). This corresponds to a reduction by 11% for the better bathymetries (HW05, Z07-ss) and up to 18 % (KK08) with respect to the 'bulk' experimental value of *Bouhifd et al*. [1996], which is $3.6 \cdot 10^{-5}$ K^{-1} (section 3.4). With steady state subsidence proportional to $\bar{\alpha}aT_m$, the lower $\bar{\alpha}$ obtained on the data set KK08 is caused by its shallower asymptotic subsidence (Figure 3). 11% is readily within the scope of the 30% explicable by rigidity in the upper lithosphere estimated by *Korenaga* [2007] (section 3.4), less than the 20% or larger reductions recently inferred [*Hillier and Watts*, 2005; *Goutorbe*, 2010], and more in line with earlier estimates (see Figure 7d) [*Parsons and Sclater*, 1977; *Stein and Stein*, 1992]. Therefore, the model refinements implemented here appear to have reduced inconsistencies related to the plate model.

4.2.2. Chablis Model

[43] Recovered parameters for the Chablis model are consistent across bathymetry data sets, apart from HW05. HW05 yields a lower T_m of 1320°C, for example, because the uncertainties on seismically derived temperatures are larger: the average $\sigma_{\bar{T}}$ is 80°C, against 45°C, for G10, as a consequence of different spatial extents. This in turn gives more weight to the fits to heat flow and bathymetry, which tend to impose lower T_m. All T_m, however, are in agreement with independent estimates of the potential temperature of the mantle (section 3.4).

[44] Asymptotic plate thicknesses a are larger than for the plate model. So are thicknesses at the age of oldest observable seafloor, 160 Myr (Table 3). These greater thicknesses, typically >125 km at 160 Myr, allow the Chablis model to match better the seismically derived temperatures around the base of the lithosphere, as they vary with age (Figure 1c). The observed vertical profiles are dependent upon lithospheric age up to depths of at least 120 km. Since modeled temperatures are constant through time beneath the thinner plate model, its visual fit to temperatures around these depths (100–120 km) is less accurate. An exception is the data set HW05, where the two models are close.

[45] The best fitting a and T_m of the Chablis model translate into a modeled heat flow at 160 Myr within 47−49 mW m^{-2}, in line with observations (Figure 1a), and a steady state heat flow in the range 21−29 mW m^{-2} (Figure 7c). Unlike the plate model, the 160 Myr value for the Chablis model is significantly greater than the steady state value because this model is still far from equilibrium for the oldest known oceanic lithosphere.

[46] *Doin and Fleitout* [1996] noted that the Chablis model needs a larger product $\bar{\alpha}T_m\sqrt{\bar{\kappa}}$ than the plate model to fit an observed topography slope at young ages, because the basal heat flow condition slows down lithospheric growth. This translates into systematically larger

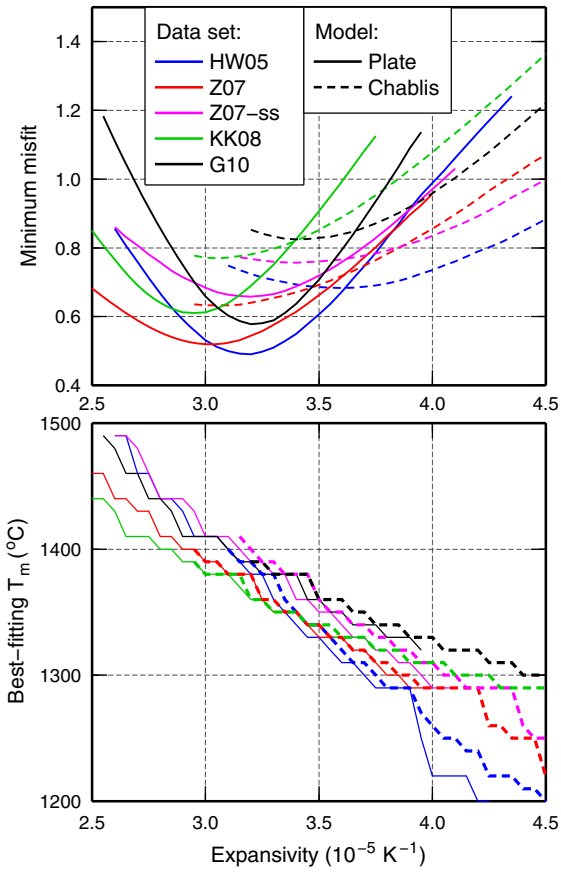

Figure 8. (top) Minimum joint misfit of the thermal models and (bottom) corresponding best-fitting T_m, function of the bulk thermal expansivity $\bar{\alpha}$.

expansivities for the former model (Table 3). These are 0 to 6% lower than the experimental values for better bathymetries (HW05, Z07-ss) and up to 15% lower for others (section 3.4).

5. Discussion

5.1. Plate Model vs. Chablis Model

[47] Both the plate and Chablis models (but not the half-space model) produce individual misfits $s_T, s_q, s_d < 1$, on all the data sets (Table 3). Given the definition of the misfit in equations (6)–(9) this indicates that these thermal models can simultaneously explain the three groups of observations within their 95% confidence intervals. This is a remarkable result, given that the incorporation of the new constraint (seismically derived temperatures) was not accompanied by any extra degree of freedom beyond the usual free parameters $(T_m, a, \bar{\alpha})$.

[48] The plate model produces the lower joint misfits, s, primarily due to its better fit to the bathymetry data (Table 3). This suggests that it may offer the most accurate framework to approximate the thermal structure and evolution of the oceanic lithosphere, in particular for constructing bathymetric reference models. This contradicts *Goutorbe*'s [2010] conclusions, but requires an acceptance that apparent values of thermal expansivity $\bar{\alpha}$ from this fitting are plausibly lowered by ~11% from experimental values by rigidity in the upper lithosphere [*Pollack*, 1980; *Korenaga*, 2007]. If, however, one chooses to impose $\bar{\alpha} = 3.6{\cdot}10^{-5}$ K^{-1} in line with the experimental values of *Bouhifd et al.* [1996] (section 3.4), Figure 8 shows that the Chablis model obtains equal (HW05, Z07, Z07-ss, G10) or lower (KK08) misfits. At the upper end of plausible experimental values ($\bar{\alpha} = 3.9{\cdot}10^{-5}$ K^{-1}) the Chablis model fits better all the data sets, with colder but equally acceptable solutions: T_m = 1290–1340°C (Figure 8, bottom). Ideally therefore independent estimates are needed on the effective value of expansivity in the oceanic lithosphere, to constrain its thermal evolution more thoroughly.

5.2. Model Adaptations

[49] The refinements made to the thermal models, described in section 3, allowed us to gain insights into the properties of the lithosphere. With the inclusion of seismically derived temperatures, and a temperature- and pressure-dependent thermal conductivity that is on average larger than previously used, the plate and Chablis models now obtain values of the potential temperature of the mantle T_m within 1320–1390°C. This result is compatible with independent constraints, without invoking an ad hoc value of radiogenic heat production to lower the fitted heat flow and the best fitting T_m (see section 4.2). However, an independent reassessment of heat production in the oceanic crust is probably necessary.

[50] The plate model yields bulk thermal expansivities $\bar{\alpha}$ not as strongly reduced as reported by recent works using similar data sets [*Hillier and Watts*, 2005; *Goutorbe*, 2010], compared to experimental data, and more in line with earlier estimates [*Parsons and Sclater*, 1977; *Stein and Stein*, 1992]. On the bathymetry curves that explicitly remove the long wavelength swells (HW05, Z07-ss, see section 2.1), $\bar{\alpha}$ is ~11% less than experimental, which is compatible with a reduction driven by rigidity of the upper lithosphere, as estimated by both *Pollack* [1980] and *Korenaga* [2007] (see section 3.4). Within the framework of the Chablis model, the best fitting $\bar{\alpha}$ are even closer to the experimental measurements; hardly any reduction is needed to fit HW05 and Z07-ss.

[51] Compared to *Goutorbe* [2010], an important refinement was to fit seismically derived temperatures at all depths up to 160 km, by downward extending the plate and Chablis models beyond their base using the adiabatic temperature profile. Although this formulation hardly affects the fit to the plate model, it significantly alters the best-fitting parameters of the Chablis model. Specifically, a fit restricted to temperatures above the (age-dependent) base of the lithosphere drives the Chablis model to lower mantle temperatures (T_m = 1110–1220°C) and consequently larger expansivities to fit ocean depths ($\bar{\alpha} = 3.75{-}4.50 \cdot 10^{-5}$ K^{-1}). However, this formulation is not self-consistent in the way it treats the subsidence and temperature observations. The model seeks to fit subsidence, which is the integrated age-dependent effect of temperature at all depths (0–160 km), yet only directly fits lithospheric temperatures. This implicitly assumes that either the temperature field does not vary with age below the base of the Chablis model, or that temperature (i.e., density) variations there do not affect surface topography, which is unlikely [e.g., *McNutt*, 1998]. For the best-fitting models without depth continuation the seismically derived temperatures that fall below the base show a clear dependence upon age (Figure 1c). Assuming isostasy above 160 km and a mean expansivity of $3.50 \cdot 10^{-5}$ K^{-1}, this dependence of sublithospheric temperature (i.e., density) on age

equates to 1–2 km of seafloor subsidence through time. This is far from negligible. The adapted model removes this bias.

5.3. Seismically Derived Temperatures vs. Bathymetry

[52] Although statistically compatible within 2σ, as indicated by the misfits s_T and $s_d < 1$, some inconsistency exists between seismically derived temperatures and bathymetry data. Bathymetry flattens (Figure 3), but seismically derived isotherms seemingly continue deepening at all ages (Figure 1d). The half-space model then best fits seismically derived temperatures, as shown by the low values of s_T in Table 3, albeit with a too high mantle temperature. Furthermore, thick, hot plates that tend toward a half-space are favored when fit to temperatures alone (Figure 7b). In other words, the price to pay for a closer fit to the temperature field is a degradation of the fit to ocean depths. The cause of the apparent incompatibility lies either with the age-depth curves, the tomography model or the velocity-temperature relationship.

[53] This study specifically included age-depth curves derived using many filtering methods from independent works (Table 2), so a systematic bias of the mean ocean depths at old ages, due to incomplete removal of features related to anomalous crust, is unlikely and the "flattening" of bathymetry curves is probably not a statistical artefact. HW05 is the most likely dataset to have been over zealous in removing bathymetric anomalies at hot spots, because it interpolates under rather than excludes features, but even this curve flattens. Seismically derived temperatures are hardly affected by the explicit exclusion of regions surrounding catalogued hot spots, implying that the continued deepening of isotherms at old ages is not caused by inclusion of anomalous temperatures.

[54] A second possibility to reconcile the seafloor flattening and seismically derived temperature data is to attribute part of the flattening to effects unrelated to the thermal structure of the lithosphere, i.e., other than small-scale convection [e.g., *Huang and Zhong*, 2005] or hot spot reheating [e.g., *Smith and Sandwell*, 1997]. Such alternative mechanisms include temporal variations in crustal thickness [*Humler et al*., 1999], lithospheric phase transitions [*Wood and Yuen*, 1983], chemical buoyancy of the mantle associated with hotspot melting [e.g., *Phipps Morgan et al*., 1995], or deeper effects related to the plate-scale mantle convection [*Davies*, 1988].

[55] In the tomography model a clear age progression of seismically derived temperatures exists below 120 km (Figure 1b), which is difficult to reconcile with plate thicknesses and could indicate vertical leakage in the upper mantle shear velocity model used here [*Shapiro and Ritzwoller*, 2002]. However vertical leakage should affect two nearly identical profiles in a very similar way, so it alone cannot cause the depth growth of isotherms and age progression of temperatures after 80–100 Myr, if one assumes that rates of change in the upper mantle structure indeed become low by such an age. A lateral leakage may explain such observations, but it implies contamination over distances much larger than the theoretical resolution of the tomography model, which varies between 350 km and 1000 km depending on the surface wave type and period [*Shapiro and Ritzwoller*, 2002].

[56] The last possibility is that the velocity-temperature relationship is incorrect. As noted in section 4.2, deep temperatures indicate a potential temperature T_{m} around 1400°C, at the upper end of petrological estimates as reevaluated by *Herzberg et al*. [2007] (section 3.4); therefore,, although particular care has been dedicated to tracking uncertainty [see *Goutorbe*, 2010], unidentified systematic effects in the velocity-temperature relationship cannot be excluded. However, an improved relationship is unlikely to fully reconcile temperatures and bathymetry, because the dependence upon age of the lithospheric structure after 80–100 Myr is encoded in the velocity model itself, so the velocity to temperature conversion simply translates this in the temperature domain. Such a dependence has long been observed from surface wave dispersion data [*Leeds et al*., 1974; *Leeds*, 1975], and the present work underlines the need for a reevaluation of its origin.

[57] In summary, no physical mechanism for the discrepancy is readily apparent, and further insight may be gained through a studies akin to this one using multiple tomographic velocity models and velocity-temperature relationships.

5.4. Beyond the Thermal Models

[58] The incompatibility between seismic tomography and subsidence data outlined in the previous section is not severe to the point of mutual exclusion of the 95% confidence intervals, as indicated by the misfits $s_T, s_q, s_d < 1$ of the plate and Chablis models. These thermal models thus allow us to force observations onto a self-consistent framework, based on the heat conduction equation (equation (2)), but they are nothing more than particular solutions of the said equation. One may question whether the basal heat supply brought by convective processes follows the simple forms prescribed by the thermal models. Of course, it is delicate to do more than fitting particular models described with a limited number of parameters using heat flow and ocean depths only, as these data simply constrain the surface derivative of the temperature field and its integral over depth, respectively. The inclusion of seismic tomography data adds constraints on the temperature field itself, and opens the possibility of setting up an inverse problem, fully independent from any particular solution of the heat equation. Such an approach may help reevaluate the nature and age-dependence of the thermal condition at base of the plate without assuming a priori a particular form, and thus gain insights into the lithosphere-asthenosphere interaction processes responsible for the basal heat supply.

6. Conclusions

[59] The thermal structure and evolution of oceanic lithosphere is optimally constrained by joint-fitting the thermal models on heat flow, several filtered age-depth curves and temperatures derived from a shear velocity model of the upper mantle. The three main cooling models are updated to all include a temperature-dependent heat capacity, a temperature- and pressure-dependent thermal conductivity, an initial condition of adiabatic decompression melting and continuity to depth. This first entirely self-consistent implementation in the context of inverting for lithospheric properties yields results that are robust to the choice of filtered bathymetry, and indicates that both basally heated models simultaneously explain the observational constraints within two standard errors. Contrastingly, the half-space model does not accurately fit any of the subsidence curves and is independently

driven to mantle potential temperatures that are too high by heat flow and seismically derived temperatures. In the detail, however, a steady state is not clearly observed in the seismically derived temperatures, whereas age-depth curves unambiguously flatten: further investigation is needed to understand the origin of this apparent incompatibility.

[60] The thermal models' set up yields lithospheric properties that are consistent with independent constraints, without invoking ad hoc effects such as radiogenic heat production to tweak the inverted data. On the global data set G10, which most closely resembles the preferred smaller sets (HW05, Z07-ss), the plate model obtains $T_m = 1390°C$, $a = 106$ km and $\bar{\alpha} = 3.20 \cdot 10^{-5} K^{-1}$, while the Chablis model yields $T_m = 1380°C$, $a = 228$ km and $\bar{\alpha} = 3.40 \cdot 10^{-5} K^{-1}$. These values correspond to steady state heat flows of 47 mW m^{-2} (plate) and 24 mW m^{-2} (Chablis). The former model better fits data jointly, thanks in large part to more accurate predicted depths, but requires an apparent thermal expansivity lower than experimental measurements; the need for such a reduction is minimal within the latter model. The preferred thermal model thus depends on its intended use and taking a view on thermal expansivity. Specifically, the plate model appears most appropriate for constructing reference bathymetry curves, but the exact nature and age-dependence of basal heat brought by deep processes is still open to question. The inclusion of seismically derived temperatures opens the possibility to make investigations that do not follow a particular solution of the heat equation, thereby allowing for a better understanding of these heating processes.

[61] **Acknowledgments.** Thoughtful reviews by M. Behn and C. Stein helped improve and clarify the manuscript. We thank Shijie Zhong, Francis Lucazeau, and Davis Hasterok for providing us their bathymetry and heat flow data.

References

Adam, C., and A. Bonneville (2005), Extent of the South Pacific Superswell, *J. Geophys. Res.*, *110*, B09408, doi:10.1029/2004JB003465.

Anderson, D. (2005), A brief history of the plume hypothesis and its competitors: Concept and controversy, in *Plates, plumes, and paradigms*, Geological Society of America Special Paper 388, edited by G. Foulger, J. Natland, D. Presnall, and D. Anderson, 303, pp. 119–145, doi:10.1130/2005.2388(08).

Anderson, D., and K. Schramm (2005), Global hotspot maps, in *Plates, Plumes and Paradigms*, edited by G. Foulger, J. Natland, D. Presnall, and D. Anderson, pp. 19–29, Geological Society of America Special Paper 388, doi:10.1130/2005.2388(03).

Artemieva, I. (2009), The continental lithosphere: Reconciling thermal, seismic, and petrologic data, *Lithos*, *109*, 23–46, doi:10.1016/j.lithos.2008.09.015.

Asaadi, N., N. M. Ribe, and F. Sobouti (2011), Inferring nonlinear mantle rheology from the shape of the Hawaiian swell, *Nature*, *473*, 501–506.

Berman, R., and L. Aranovich (1996). Optimized standard state and solution properties of minerals: 1. model calibration for olivine, orthopyroxene, cordierite, garnet, and ilmenite in the system FeO-MgO-CaO-Al_2O_3-TiO_2-SiO_2, *Contrib. Mineral. Petrol.*, *126*, 1–24, .

Bouhifd, M., D. Andrault, G. Fiquet, and P. Richet (1996),Thermal expansion of forsterite up to the melting point, *Geophys. Res. Lett.*, *23*(10), 1143–1146.

Caress, D. W., M. K. McNutt, R. S. Detrick, and J. C. Mutter (1995), Seismic Imaging of Hot spot-Related Underplating Beneath the Marquesas Islands, *Nature*, *373*, 600–603.

Coffin, M., and O. Eldholm (1994) Large igneous provinces: Crustal structure, dimensions, and external consequences, *Rev. Geophys.*, *32*, 1–36.

Crosby, A. G., D. McKenzie, and J. G. Sclater (2006), The Relationship Between Depth, Age and Gravity in the Oceans, *Geophys. J. Int.*, *166*, 553–573.

Crough, S. (1975), Thermal model of oceanic lithosphere, *Nature*, *256*, 388–390.

Crough, S., (1978), Thermal origin of mid-plate hot-spot swells, *Geophys. J. R. Astr. Soc.*, *55*, 451–469.

Crough, S., and G. Thompson (1976), Numerical and approximate solutions for lithospheric thickening and thinning, *Earth Planet. Sci. Lett.*, *31*, 397–402.

Davaille, A., and C. Jaupart (1994), Onset of thermal convection in fluids with temperature-dependent viscosity: Application to the oceanic mantle, *J. Geophys. Res.*, *99*(B10), 19,853–19,866.

Davies, G. (1988), Ocean bathymetry and mantle convection, 1. Large-scale flow and hotspots, *J. Geophys. Res.*, *93*(B9), 10,467–10,480.

Davis, E., and C. Lister (1974), Fundamentals of ridge-crest topography, *Earth Planet. Sci. Lett.*, *21*, 405–413.

DeLaughter, J., S. Stein, and C. Stein (1999), Extraction of a lithospheric cooling signal from oceanwide geoid data, *Earth Planet. Sci. Lett.*, *174*, 173–181.

Denlinger, R. P. (1992), A Revised Estimate for the Temperature Structure of the Oceanic Lithosphere, *J. Geophys. Res.*, *97*(B5), 7219–7222.

Detrick, R., and S. Crough (1978), Island subsidence, hot spots, and lithospheric thinning, *J. Geophys. Res.*, *83*(B3), 1236–1244.

Divins, D. (2011), NGDC total sediment thickness of the world's oceans and marginal seas, http://www.ngdc.noaa.gov/mgg/sedthick/sedthick.html.

Doin, M., and L. Fleitout (1996), Thermal evolution of the oceanic lithosphere: an alternative view, *Earth Planet. Sci. Lett.*, *142*, 121–136.

Elderfield, H., K. Becker, and E. Davis (2004), Foundations of research into heat, fluid, and chemical fluxes in oceanic crust, in *Hydrogeology of the Oceanic Lithosphere*, edited by E. Davis and H. Elderfield, pp. 28–56, Cambridge University Press, Cambridge, U.K.

Fei, Y., and S. Saxena (1986), A thermochemical data base for phase equilibria in the system Fe-Mg-Si-O at high pressure and temperature, *Phys. Chem.Miner.*, *13*, 311–324.

Gibert, B., U. Seipold, A. Tommasi, and D. Mainprice (2003), Thermal diffusivity of upper mantle rocks: Influence of temperature, pressure, and the deformation fabric, *J. Geophys. Res.*, *108*(B8), 2359, doi:10.1029/2002JB002108.

Gibert, B., F. Schilling, K. Gratz, and A. Tommasi (2005), Thermal diffusivity of olivine single crystals and a dunite at high temperature: Evidence for heat transfer by radiation in the upper mantle, *Phys. Earth Planet. Inter.*, *151*, 129–141, doi:10.1016/j.pepi.2005.02.003.

Gillet, P., P. Richet, F. Guyot, and G. Fiquet (1991), High temperature thermodynamic properties of forsterite, *J. Geophys. Res.*, *96*(B7), 11,805–11,816.

Goes, S., R. Govers, and P. Vacher (2000), Shallow mantle temperatures under europe from *P* and *S* wave tomography, *J. Geophys. Res.*, *105*(B5), 11,153–11,169.

Goutorbe, B. (2010), Combining seismically derived temperature with heat flow and bathymetry to constrain the thermal structure of oceanic lithosphere, *Earth Planet. Sci. Lett.*, *295*, 390–400, doi:10.1016/j.epsl.2010.04.013.

Heestand, R., and S. Crough (1981), The effect of hot spots on the oceanic age-depth relation, *J. Geophys. Res.*, *86*, 6107–6114.

Herzberg, C., P. Asimow, N. Arndt, Y. Niu, C. Lesher, J. Fitton, M. Cheadle, and A. Saunders (2007), Temperatures in ambient mantle and plumes: Constraints from basalts, picrites, and komatiites, *Geochim. Geophys. Geosyst.*, *8*(2), Q02006, doi:10.1029/2006GC001390.

Hillier, J., and A. Watts (2004), "Plate-like" subsidence of the East Pacific Rise–South Pacific superswell system, *J. Geophys. Res.*, *109*, B10102, doi:10.1029/2004JB003041.

Hillier, J., and A. Watts (2005), Relationship between depth and age in the North Pacific Ocean, *J. Geophys. Res.*, *110*, B02405, doi:10.1029/2004JB003406.

Hofmeister, A. (1999), Mantle values of thermal conductivity and the geotherm from phonon lifetimes, *Science*, *283*, 1699–1706.

Honda, S., and D. Yuen (2001), Interplay of variable thermal conductivity and expansivity on the thermal structure of oceanic lithosphere, *Geophys. Res. Lett*, *28*(2), 351–354.

Huang, J., and S. Zhong (2005), Sublithospheric small-scale convection and its implications for the residual topography at old ocean basins and the plate model, *J. Geophys. Res.*, *110*, B05404, doi:10.1029/2004JB003153 .

Humler, E., C. Langmuir, and V. Daux (1999), Depth versus age: new perspectives from the chemical compositions of ancient crust, *Earth Planet. Sci. Lett.*, *173*, 7–23.

Jaupart, C., and J. Mareschal (2007), Heat flow and thermal structure of the lithosphere, in *Treatise on geophysics, Vol. 6: Crust and lithosphere dynamics*, edited by A. Watts, pp. 217–251, Elsevier, Amsterdam.

Jordan, T. H. (1979), Mineralogies, densities and seismic velocities of garnet lherzolites and their geophysical implications, in *The Mantle Sample: Inclusions in Kimberlites and Other Volcanics*, edited by F. R. Boyd and H. O. A. Meyer, pp. 1–14, Americal Geophysical Union, Washington, D.C.

Karato, S. (1993), Importance of anelasticity in the interpretation of seismic tomography, *Geophys. Res. Lett.*, *20*(15), 1623–1626.

Katsura, T., et al. (2004), Olivine-wadsleyite transition in the system (mg, fe)$_2$sio$_4$, *J. Geophys. Res.*, *109*, B02209, doi:10.1029/2003JB002438.

Katz, R., M. Spiegelman, and C. Langmuir (2003), A new parameterization of hydrous mantle melting, *Geochim. Geophys. Geosyst.*, *4*(9), 1073, doi:10.1029/2002GC000433

Korenaga, J. (2007), Effective thermal expansivity of maxwellian oceanic lithosphere, *Earth Planet. Sci. Lett.*, *257*, 343–349, doi:10.1016/j.epsl.2007.03.010.

Korenaga, T., and J. Korenaga (2008), Subsidence of normal oceanic lithosphere, apparent thermal expansivity, and seafloor flattening, *Earth Planet. Sci. Lett.*, *268*, 41–51, doi:10.1016/j.epsl.2007.12.022.

Laske, G., and G. Masters (1997), A global digital map of sediment thickness, *EOS Trans. AGU*, *78*, F483.

Leeds, A. (1975), Lithospheric thickness in the western Pacific, *Phys. Earth Planet. Inter.*, *11*, 61–64.

Leeds, A., L. Knopoff, and E. Kausel (1974), Variations of upper mantle structure under the Pacific Ocean, *Science*, *186*(4159), 141–143.

Lister, C. R. B. (1974), Penetration of water into hot rock, *Geophys. J. R. Astron. Soc.*, *39*, 465–509.

Malinverno, A. (1990), A quantitative study of the axial topography of the Mid-Atlantic Ridge, *J. Geophys. Res*, *95*(B3), 2645–2660.

Marks, K. M., and D. T. Sandwell (1991), Analysis of Geoid Height Versus Topography for Oceanic Plateaus and Swells Using Non-Biased Linear-Regression, *J. Geophys. Res.*, *96*(B5), 8045–8055.

McKenzie, D. (1967), Some remarks on heat flow and gravity anomalies, *J. Geophys. Res.*, *72*(24), 6261–6273.

McKenzie, D. (1984), The Generation and Compaction of Partially Molten Rock, *J. Petrol.*, *25*, 713–763.

McKenzie, D., J. Jackson, and K. Priestley (2005), Thermal structure of oceanic and continental lithosphere, *Earth Planet. Sci. Lett.*, *233*, 337–349, doi:10.1016/j.epsl.2005.02.005.

McNutt, M. (1998), Superswells, *Rev. Geophys.*, *36*(2), 211–244.

McNutt, M., and A. V. Judge (1990), The Superswell and Mantle Dynamics Beneath the South Pacific, *Science*, *248*, 969–975.

McNutt, M. K. (1995), Marine Geodynamics: Depth-Age Revisited, *Rev. Geophys.*, *33*(Part 1 Suppl. S), 413–418.

Moore, W. B., and G. Schubert (1997), Lithospheric Thinning and Chemical Buoyancy Beneath the Hawaiian Swell, *Geophys. Res. Lett.*, *24*(11), 1287–1290.

Müller, R., M. Sdrolias, C. Gaina, and W. Roest (2008), Age, spreading rates, and spreading asymmetry of the world's ocean crust, *Geochim. Geophys. Geosyst.*, *9*, Q04,006, doi:10.1029/2007GC001743.

Niu, Y., C. Langmuir, and R. Kinzler (1997), The origin of abyssal peridotites: a new perspective, *Earth Planet. Sci. Lett.*, *152*, 251–265.

Parsons, B., and D. McKenzie (1978), Mantle convection and the thermal structure of the plates, *J. Geophys. Res.*, *83*(B9), 4485–4496.

Parsons, B., and J. Sclater (1977), An analysis of the variation of ocean floor bathymetry and heat flow with age, *J. Geophys. Res.*, *82*(5), 803–827.

Phipps Morgan, J., W. Morgan, and E. Price (1995), Hotspot melting generates both hotspot volcanism and a hotspot swell? *J. Geophys. Res.*, *100*(B5), 8045–8062.

Pollack, H. (1980), On the use of the volumetric thermal expansion coefficient in models of ocean floor topography, *Tectonophysics*, *64*, T45–T47.

Pollack, H., S. Hurter, and J. Johnson (1992), Global heat flow data set, *Tech. rep.*, World Data Center A for Solid Earth Geophysics, NOAA E/GCI, 325 Broadway, Boulder, CO 80303, USA.

Pratt, J. H. (1859), On the Deflection of the Plumb-Line in India, Caused by the Attraction of the Himalaya Mountains and of the Elevated Regions Beyond; and its Modification by the Compensating Effect of a Deficiency of Matter Below the Mountain-Mass, *Philos. Trans. R. Soc. London*, *149*, 745–796.

Ritzwoller, M., N. Shapiro, and S.-J. Zhong (2004), Cooling history of the pacific lithosphere, *Earth Planet. Sci. Lett.*, *226*, 69–84.

Schatz, J., and G. Simmons (1972), Thermal conductivity of earth material at high temperature, *J. Geophys. Res.*, *77*(33), 6966–6983.

Sclater, J., R. Anderson, and M. Bell (1971), Elevation of ridges and evolution of the Central Eastern Pacific, *J. Geophys. Res.*, *76*(32), 7888–7915.

Shapiro, N., and M. Ritzwoller (2002), Monte-carlo inversion for a global shear-velocity model of the crust and upper mantle, *Geophys. J. Int.*, *151*, 88–105.

Sleep, N. (2006), Mantle plumes from top to bottom, *Earth Sci. Rev.*, *77*(4), 231–271, doi:10.1016/j.earscirev.2006.03.007.

Smith, W., and D. Sandwell (1997), Global sea floor topography from satellite altimetry and ship depth soundings, *Science*, *277*, 1956–1962.

Sobolev, S., H. Zeyen, G. Stoll, F. Werling, R. Altherr, and K. Fuchs (1996), Upper mantle temperatures from teleseismic tomography of french massif central including effects of composition, mineral reactions, anharmonicity, anelasticity and partial melt, *Earth Planet. Sci. Lett.*, *139*, 147–163.

Stein, C., and S. Stein (1992), A model for the global variation in oceanic depth and heat flow with lithospheric age, *Nature*, *359*, 123–129.

Stein, C., and S. Stein (1994), Constraints on hydrothermal heat flux through the oceanic lithosphere from global heat flow, *J. Geophys. Res.*, *99*(B2), 3081–3096.

Thoraval, C., A. Tommasi, and M.-P. Doin (2006), Plume-lithosphere interaction beneath a fast moving plate, *Geophys. Res. Lett.*, *33*, L01301, doi:10.1029/2005GL024047.

Turcotte, D., and E. Oxburgh (1967), Finite amplitude convective cells and continental drift, *J. Fluid Mech.*, *28*, 29–42.

Watts, A. B., D. P. McKenzie, B. E. Parsons, and M. Roufosse (1985), The Relationship Between Gravity and Bathymetry in the Pacific Ocean, *Geophys. J. R. Astron. Soc.*, *83*, 263–298.

Wessel, P. (2001), Global distribution of seamounts inferred from gridded Geosat/ERS-1 altimetry, *J. Geophys. Res.*, *106*(B9), 19,431–19,441.

White, R. S., and D. McKenzie (1995), Mantle Plumes and Flood Basalts, *J. Geophys. Res.*, *100*(B9), 17,543–17,585.

White, R. S., D. McKenzie, and R. K. O'Nions (1992), Oceanic Crustal Thickness from Seismic Measurements and Rare-Earth-Element Inversions, *J. Geophys. Res.*, *97*, 19,683–19,715.

Wood, B. J., and D. A. Yuen (1983), The role of lithospheric phase transitions on seafloor flattening at old ages, *Earth Planet. Sci. Lett.*, *66*, 303–314.

Yan, B., E. Graham, and K. Furlong (1989), Lateral variations in upper mantle thermal structure inferred from three-dimensional seismic inversion models, *Geophys. Res. Lett.*, *16*(5), 449–452.

Zhong, S., M. Ritzwoller, N. Shapiro, W. Landuyt, J. Huang, and P. Wessel (2007), Bathymetry of the pacific plate and its implications for thermal evolution of lithosphere and mantle dynamics, *J. Geophys. Res.*, *112*, B06412, doi:10.1029/2006JB004628.